

DTI Connectivity by Segmentation

Marc Niethammer[†], Alexis Boucharin[†], Christopher Zach⁺,
Eric Maltbie[†], Mar Sanchez^{*}, Martin Styner[†]

[†]University of North Carolina at Chapel Hill, ^{*}Emory University
⁺Swiss Federal Institute of Technology (ETH) Zurich

Abstract. This paper proposes a new method to compute connectivity information from diffusion weighted images. It is inspired by graph-based approaches to connectivity definition, but formulates the estimation problem in the continuum. In particular, it defines the connectivity through the minimum cut in tensor-weighted space. It is therefore closely related to prior work on segmentation using continuous versions of graph cuts. A numerical solution based on a staggered grid is proposed which allows for the computation of flux directly through diffusion tensors. The resulting global connectivity measure is the maximum diffusive flow supported between two regions of interest.

1 Introduction

Diffusion weighted magnetic resonance imaging (DW-MRI) can be used to measure local water diffusion in tissues in vivo. Local diffusion information is commonly used to infer connectivity information (for example in the brain) through tractography. Connectivity measures have been defined using streamline tractography, probabilistic tractography [1], optimal path approaches [2], or by geodesics in a tensor-warped space [3]. One of the major shortcomings of classical streamline tractography is its sensitivity to noise, due to the random drift occurring during the underlying integration process and due to regions with ambiguous orientation information. Probabilistic tractography alleviates the problem of orientation ambiguity by sampling large numbers of fibers, but it is still based on streamline tractography. Optimal path approaches on the other hand approach the tractography problem by finding the shortest path between two regions of interest. This is conceptually nice, because the solution space is better constrained, however, in practice these methods are prone to taking shortcuts, which requires tight control through masking to obtain anatomically meaningful connections.

Zalesky et al. [4] recently defined a connectivity measure by computing the maximum flow through a graph. They identify three desirable properties, which do not hold for standard connectivity measures: 1) independence to length of the connection, 2) proportionality to bundle cross-sectional area, and 3) invariance of the measure under exchange of source and target regions.

The approach developed in this paper is inspired by [4]. However it formulates the solution in the continuum (removing the need for graph construction) and uses the full tensor information (opposed to only the direction of the major eigenvector) for the connectivity computation. This paper is not concerned

with finding the actual path, but rather the maximally supported flow between two regions of interest using a tensor-valued metric is computed. More general measures could easily be incorporated into the framework. The proposed method constitutes a continuous tensorial version of a minimum cut/maximum flow computation and is related to recent work in image segmentation [5,6].

Major advantages of the proposed method over previous work are: (i) The method allows for the easy integration of tensor information (which is much harder for a standard graph-based solution) and is extensible to more general descriptions of diffusion. (ii) The method is essentially parameter-free and directly computes a physically meaningful quantity which can be used as a surrogate measure for connectivity. (iii) The associated optimization problem can be solved reliably, because it is convex and therefore the globally optimal solution can be computed.

Sec. 2 formulates the segmentation problem. Sec. 3 discusses the numerical solution. Synthetic and real results are presented in Sec. 4. Sec. 5 concludes with an outlook on future work.

2 Segmentation/Maximum-Flow Problem

One of the simplest diffusion models is the diffusion tensor which relates local diffusion properties to measured DW signals through the Stejskal-Tanner equation

$$S_k = S_0 e^{-bg_k^T \mathcal{D} g_k},$$

where b is the b-value, g_k are the gradient directions, S_0 is the baseline image, S_k are the diffusion weighted images, and \mathcal{D} denotes the diffusion tensor. $\mathcal{D}g_k$ can be interpreted as the diffusive flux according to Fick's law of diffusion. A global measure of connectivity between two regions of interest, which fulfills the properties given by Zalesky [4] can then be defined as the maximal diffusive flow between the two regions according to Fick's law.

Given a source (\mathcal{S}) and a target (\mathcal{T}) region, the maximal diffusive flow by an underlying tensor field assuming an incompressible fluid without internal sources or sinks can be obtained by solving the segmentation problem associated with minimizing the energy

$$E(u) = \int \|\mathcal{D}\nabla u\| dx, \quad x \in \Omega, \quad u \in \{0, 1\}, \quad u(x) = 1 \quad \forall x \in \mathcal{S}; \quad u(x) = 0 \quad \forall x \in \mathcal{T}, \quad (1)$$

where u is an indicator function, labeling voxels between the cut and the source with 1, and 0 everywhere else, and $\Omega \subset \mathbb{R}^3$ is the domain of definition (in this setting typically given by a white matter mask), $\mathcal{S}, \mathcal{T} \subset \Omega$. The discontinuity set of the optimal solution

$$u^* = \underset{u}{\operatorname{argmin}} E(u),$$

can be considered the tensor-valued, continuous equivalent of a minimum cut in a graph. The maximum diffusive flow is the flux integrated across this discontinuity set or more simply the energy value at the optimum, i.e., $E(u^*)$.

Note that an approach to tractography and connectivity information based on the diffusive flux (Fick’s law) has been previously proposed by O’Donnell [3]. However, in this case the (implied) optimization problem is to minimize

$$E(u) = \frac{1}{2} \int \|\mathcal{D}^{\frac{1}{2}} \nabla u\|^2 dx, \quad x \in \Omega, \quad u \in \mathbb{R}, \quad u(x) = 1 \quad \forall x \in \mathcal{S}; \quad u(x) = 0 \quad \forall x \in \mathcal{T}.$$

This results in a smooth concentration field which can be used to define correspondences between source and target. A connectivity measures can then be defined by integrating the flux along the correspondence trajectories between source and target. In contrast, the minimization of Eq. 1 results directly in a measurement of the *maximal flow* by integrating the flux over the discontinuity set (the tensor-weighted total variation) with $u \in \{0, 1\}$. There is no need to explicitly compute the correspondences.

The energy 1 is non-convex, because the domain of u is a non-convex set. However, relaxing the condition on u to $u \in [0, 1]$ results in a convex optimization problem [6]. See also [5,7] for segmentation methods using isotropic metrics. Despite this relaxation, the solutions obtained for u are essentially binary [6], i.e., any segmentation obtained by thresholding u^* at a value $\theta \in (0, 1)$ will be globally optimal. The discontinuity set indicates the location of the minimum cut. The energy is also directly related to anisotropic total variation regularization [8].

The relaxed problem can be solved by the equivalent minimax problem

$$\{u^*, p^*\} = \arg \min_u \max_p \int p^T \mathcal{D} \nabla u \, dx, \quad \|p\| \leq 1 \quad u \in [0, 1]. \quad (2)$$

The dual energy is

$$E_{dual} = - \int_S \operatorname{div}(\mathcal{D}^T p) \, dx + \int_{\overset{\circ}{\Omega}} \min(0, \operatorname{div}(\mathcal{D}^T p)) \, d\overset{\circ}{\Omega},$$

where $\overset{\circ}{\Omega}$ denotes all voxels which are neither source nor target voxels. The dual energy can be used to assess the quality of a current solution iterate, since it is a tight lower bound on the energy [9].

While increased flow values may be obtained due to the inclusion of flux contributions of anatomically questionable fibers, the result of the method is (in contrast to optimal path methods) not dominated by potential shortcuts. Instead, the value of the maximum flow will be dominated by the influence of the strongest connection between source and target. Note that a major advantage of the proposed method is that it is completely parameter-free unlike standard methods based on streamline tractography, which typically have parameters controlling step-size, curvature, minimal and maximal length, integration method used, etc.

3 Numerical Considerations

The gradient descent scheme to solve 2 is

$$u_\tau = \operatorname{div}(\mathcal{D}^T p) \quad p_\tau = \mathcal{D} \nabla u, \quad \|p\| \leq 1, \quad u \in [0, 1], \quad (3)$$

which is known as the Arrow-Hurwitz-Uzawa method [10]. Implementation requires the computation of the divergence of the transformed dual variables p as well as the gradient of the indicator function u . To measure flow through tensors at the location where the tensors are defined the gradient operator should be chosen such that it is evaluated colocated with p . This is achieved by a staggered grid, as depicted in Fig. 1¹. Using trilinear interpolation (for an image volume – assuming for presentational simplicity isotropic voxels) for the indicator variables surrounding a dual variable

$$u(x + dx, y + dy, z + dz) = (1 - dx)(1 - dy)(1 - dz)u(x, y, z) + dx(1 - dy)(1 - dz)u(x + 1, y, z) + \dots; \quad dx, dy, dz \in [0, 1],$$

the gradient is simply the average of the gradients in the respective spatial directions, i.e.,

$$(u_x)_{i+\frac{1}{2}, j+\frac{1}{2}, k+\frac{1}{2}} = \frac{1}{4} \sum_{a, b \in \{0, 1\}^2} (u_{i+1, j+a, k+b} - u_{i, j+a, k+b}),$$

and similarly for the other spatial directions. The spatial derivatives for the divergence operator need to be chosen such that it is the adjoint of the gradient operator for u , therefore

$$(p_x)_{i, j, k} = \frac{1}{4} \sum_{a, b \in \{-\frac{1}{2}, \frac{1}{2}\}^2} (p_{i+\frac{1}{2}, j+a, k+b} - p_{i-\frac{1}{2}, j+a, k+b}),$$

and similarly for the other spatial directions, so that $div(p) = p_x + p_y + p_z$. The dual variables p are defined strictly inside the domain of the indicator variables u (as illustrated in Fig. 1). The derivatives of p at the boundary of the domain are computed such that values for p for indices outside the domain are set to zero. These are the natural boundary conditions for $-div(\cdot)$ to be adjoint to ∇ on the staggered grid.

Using a modified gradient descent for saddlepoint problems due to Popov [11] instead of the direct scheme 3 accelerates convergence. This is a fast primal-dual iteration scheme, which was used successfully by Pock et al. [12] for the minimization of the Mumford-Shah functional. The algorithm for the tensor-valued case is given in Fig. 2.

4 Results

Sec. 4.1 shows the performance of the algorithm on synthetic experiments and compares results to [4]. Sec. 4.2 applies the algorithm to a set of DT-MR images of macaques at age 2 weeks and 6 months.

¹ When defining both the gradient and the divergence operator on the same grid, for example by forward and backward differences respectively, the solution becomes asymmetric. Further, the minimum cut will lie in-between voxels, instead of cutting through their centers. The staggered grid avoids this undesirable behavior.

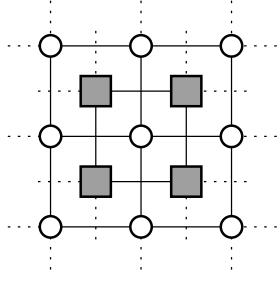


Fig. 1. Illustration of the principle of the staggered grid. Flow vectors p are defined at the location of the gray squares, indicator variables u are defined at the locations of the circles. Consequentially, gradients are defined on the squares and divergence on the circles. This allows for computation of flow through the tensors themselves.

Data: Seed points, tensor field \mathcal{D}

Result: Indicator function u , flow field p , maximum-flow value μ

Transfer the seedpoints from original grid to the staggered grid ;

Initialize source and target points with $u = 1$ and $u = 0$; other points to $u = \frac{1}{2}$;

Initialize $p = 0$, $u_a = u$, $u_b = u$;

repeat

 Compute gradient: $g = \nabla u_b$;

 Update flow field: $p = p + \tau \mathcal{D}g$;

 Ensure $\|p\| \leq 1$: $p = p / (\max(1, \|p\|))$;

 Compute divergence: $d = \text{div}(\mathcal{D}^T p)$;

 Update u : $u_a = u + \tau d$; $u_b = 2u_a - u$; $u = u_a$;

 Compute relative duality gap: $\Delta = \frac{\text{energy-dual energy}}{\text{energy}}$

until convergence ($\Delta \leq \theta$) ;

μ is $\int \|\mathcal{D}\nabla u\| d\Omega$.

Algorithm 1: Primal-dual solution method.

Fig. 2. Algorithmic description of the primal-dual method of [12] as applied to the tensor-segmentation case.

4.1 Synthetic experiments

A simple two-dimensional synthetic example for crossing fibers, illustrated in Fig. 3, shows the behavior of the algorithm under noise and directional ambiguities (due to crossings under the diffusion tensor model). The noise-free tensors were chosen as

$$T_1 = \frac{1}{1000} \begin{pmatrix} 3 & 0 \\ 0 & 1 \end{pmatrix} \quad \text{and} \quad T_2 = \frac{1}{1000} \begin{pmatrix} 1 & 0 \\ 0 & 3 \end{pmatrix}$$

respectively. The eigenvalues of the tensors for the vertical strip were weighted by a scaling factor $f \in [0, 1]$ and tensors were combined in the overlapping region by selecting the maximum eigenvalues of the two tensors in both directions. To add noise, DWIs were computed with b-value $b = 1000$, baseline intensity $S_0 = 1000$ from the tensors at degrees $\{0, 22.5, 45, 67.5, 90\}$ (defining the two-dimensional gradient directions) in the plane. Rician noise with varying σ was subsequently added. Least-squares tensor estimation resulted in a noisy-tensor. Tensors are zero outside the crossing strips.

A set of experiments was performed combining noise levels for $\sigma \in [0, 100]$ and crossing fractions $f \in [0, 1]$. Fig. 5 shows the mean and the standard deviation

tion for the computed maximum flow values for a set of 25 random repetitions of the experiments over the complete range for f and σ . The exact value for the noise-free experiment is $45e - 3$ (obtained by integrating the diffusive flux over a cross section), which is matched by the computed value in the noise-free case. While the computed flow value decreases with increases in the noise level (noise causes tensors to reorient, resulting in an overall decrease of diffusive flow as illustrated in Fig. 4), its value is consistent with changes in the crossing fraction. Estimation accuracy over the 25 repetitions is high, however an increase in estimation variance is observed for increases in noise level.

To compare the results to other methods in the literature, Fig. 6 shows results for the (recreated) synthetic Archimedian spiral by Zalesky and Fornito [4]. The synthetic dataset consists of noisy cigar-shaped tensors, which are aligned with the tangent of the Archimedean spiral and isotropic tensors at a given distance away from the spiral. See [4] for details on the dataset. DWIs for thirty gradient directions were generated for an image resolution of $256 \times 256 \times 14$. No partial volume modeling (as in [4]) was used, instead the algorithm runs directly on the original (not upsampled) grid, using a mask with 4 mm radius around the center of the spiral. Fig. 6 shows maximum flow estimation results for radii of the spiral of 1, 2, 3 and 4 mm respectively. Results represent computations between an initial source point and 9 target points distributed evenly over the spiral. The result of a good method should show increased connectivity measures for increases in radius, because this corresponds to a larger number of fibers and therefore a stronger connection. A method should also show essentially flat connectivity profiles when sampled along different points of the path, indicating invariance to the length of the path. The proposed algorithm yields highly consistent estimation results. Fig. 7 shows the normalized connectivity profiles (with a connectivity of 1 at the source location) obtained from the results in [4] for the method proposed in [4], for FSL [13], and for FSL with compensation for length bias in comparison to the maximum flow method of this paper. The maximum flow method clearly outperforms the other methods in terms of estimation consistency, obtaining a almost perfectly flat connectivity profile along the spiral.

4.2 Experiments on real datasets

The proposed method was applied to scans from an ongoing study of neurodevelopmental alterations caused by infant maltreatment in rhesus monkeys. Six selected rhesus macaques were scanned longitudinally. Data from 2 weeks old subjects (neonates) and 6 months old subjects was analyzed. Scans were acquired on a 3T Siemens Trio scanner with 8-channel phase array trans-receiving volume coil. High-resolution T1-weighted and T2 weighted MRI scans were acquired first, followed by the DTI scans (voxel size: $1.3 \times 1.3 \times 1.3 \text{ mm}^3$ with zero gap, 60 directions, TR/TE=5000/86 ms, 40 slices, FOV: 83 mm, b:0, 1000 s/mm², 12 averages). These datasets were selected as they have SNR values at low (at 2 weeks) and intermediate (6 months) level.

An expert rater, trained in streamline fiber tractography, determined source and target regions that produced valid DTI fiber tracts for the corpus callo-

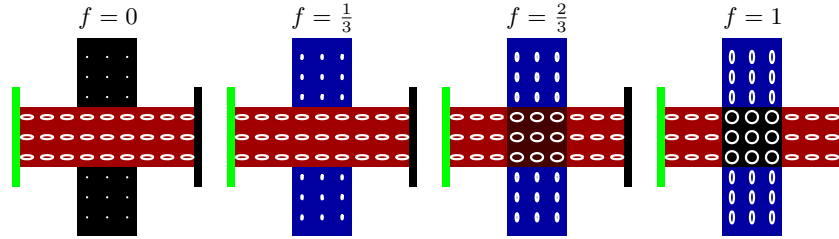


Fig. 3. Noise-free crossing case for different crossing fractions. The green and the black bars indicate the source and the target regions respectively. The red and blue colors are the planar equivalents of color-by-orientation plots, where blue denotes flow in the up/down-direction and red in the left/right direction. The intensity is modulated by fractional anisotropy of the underlying tensor.

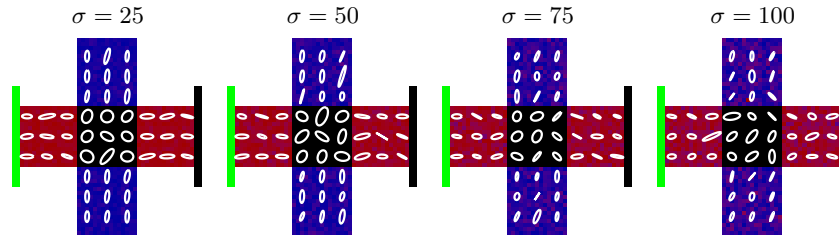


Fig. 4. Noisy crossing case, to illustrate the noise magnitudes applied.

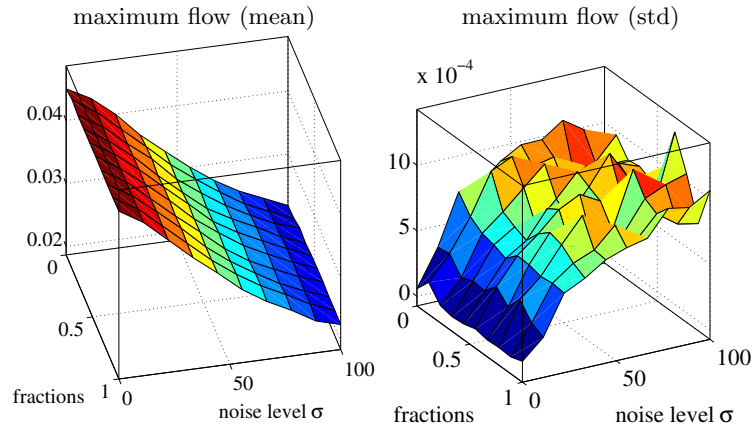


Fig. 5. Mean energy values (left) and their standard deviation (right) for 25 repetitions of 100 different σ /fraction pairings for the synthetic crossing dataset. Maximum flow decreases with increases in noise level, but is highly consistent under changes in crossing fraction.

sum genus, the splenium tracts, and for the internal capsule motor tract (see Fig. 8 for an illustration). Corresponding source and target regions were used to

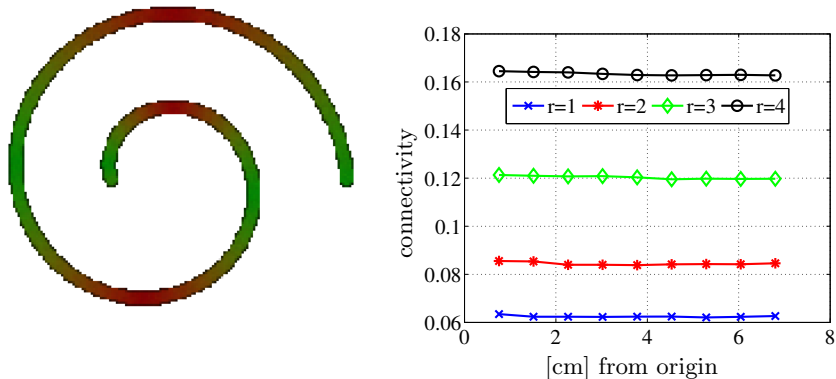


Fig. 6. Synthetic spiral as proposed in [4] (left). Estimation results for varying radii of the spiral (right; 1, 2, 3, 4 mm radius, bottom to top) for increasing distances of the target region from the source region along the spiral.

compute the proposed connectivity values (see Tab. 9). Connectivity computations were restricted to an expert-generated white matter mask, obtained by FA thresholding. From Tab. 9 several conclusions can be drawn: a) as expected the internal capsule has higher connectivity values than the splenium and the genu, b) splenium and genu have more similar values, but the genu is slightly higher (again expected), c) with the exception of the splenium a connectivity increase from 2 weeks to 6 months is visible, d) surprisingly the inter-subject variability is higher than the longitudinal changes.

In summary, while the tests indicated limitations of the method mainly with respect to inter-subject variability (for the dataset used), the results also point to the potential use of the maximal flow connectivity measure as an alternative to existing, tractography based connectivity measures.

5 Conclusion and Future Work

This paper described a global method to compute connectivity measures from DTI. It can be viewed as a continuous version of the approach by Zalesky [4], but additionally makes use of a tensor’s diffusion strength. While the method is described in terms of the tensor model, it can be generalized to more general descriptions of diffusion. Unlike many other methods, the computed results are not based on the explicit computation of streamlines. However, a flow-field is constructed internally (given by the dual variable). Since this flow field is not unique it is not a replacement for streamline tractography at this stage. However, the computed maximum flow value is globally optimal (identical for all optimal flow fields), can be reliably obtained due to the underlying convex optimization problem of the method, and can be used as a surrogate measure for connectivity. An interesting future research direction is to construct admissible flow fields which adhere as much as possible to the underlying tensor-field, while preserving

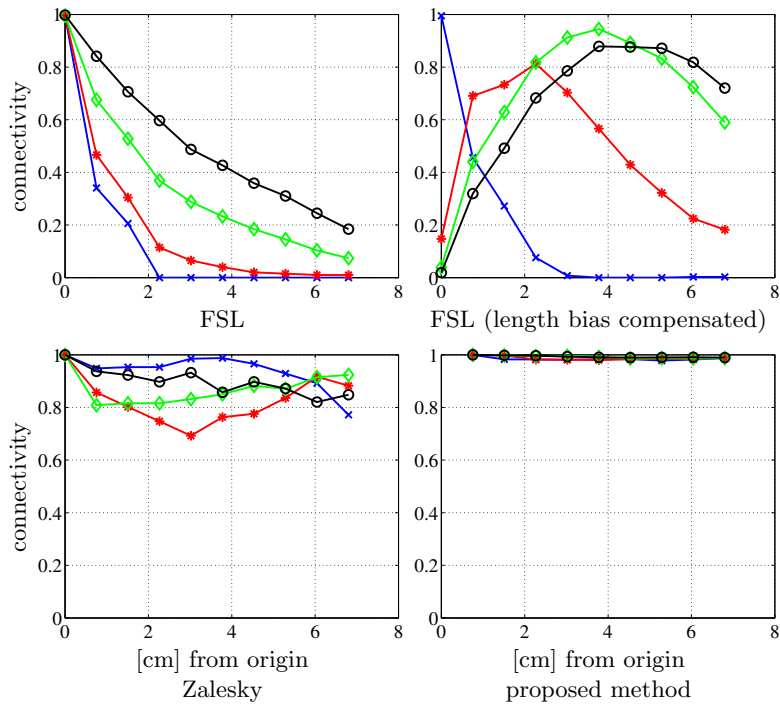


Fig. 7. Connectivity-normalized synthetic simulation results. Comparisons with FSL, FSL (length bias compensated), and Zalesky’s method recreated from data of [4]. Symbols indicate spiral radius as in Fig. 6. The proposed method produces the most consistent estimation results.

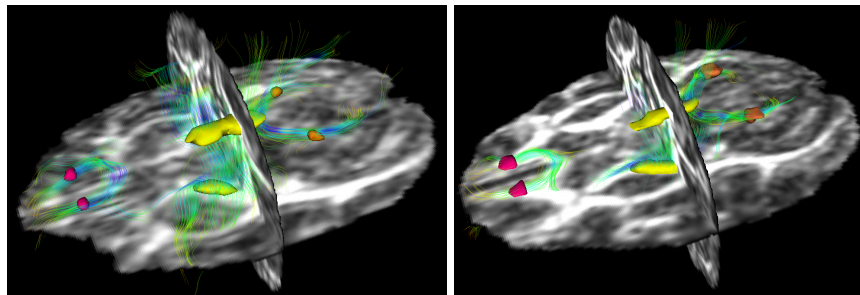


Fig. 8. ROI for the genu (pink), splenium (orange) and the internal capsule motor tracts (yellow) shown on the FA maps for the 2 weeks (left) and 6 months (right) monkey data. Fiber tracts from standard streamline method were shown to highlight the ROI, but are not used in the proposed method.

the flow magnitude and direction at the location of the minimum cut. This would allow for the reconstruction of flow fields (and fibers) through ambiguous regions.

Fig. 9. Global connectivity values (mean and standard deviation) for 3 selected fiber tract regions in rhesus macaques at age 2 weeks and 6 months.

Tract Name	2 weeks		6 months	
	Mean	Stdev	Mean	Stdev
Genu	0.051	0.008	0.057	0.003
Splenium	0.040	0.015	0.040	0.020
Internal Capsule	0.125	0.026	0.136	0.027

Acknowledgements This material is based upon work supported by the National Science Foundation (NSF) under Grant No. (EECS-0925875), by the National Institutes of Health (NIH) under Grant Nos. (R21 HD55255-2, U54 EB005149-01, RC1AA019211-01, P50 MH078105, P50 MH078105-01A2S1, R42 NS059095-03) and by UNC IDDRC HD 03110. Any opinions, findings, and conclusions or recommendations expressed in this material are those of the author(s) and do not necessarily reflect the views of NSF or NIH.

References

- Behrens, T.E.J., Woolrich, M.W., Jenkinson, M., Johansen-Berg, H., Nunes, R.G., Clare, S., Matthews, P.M., Brady, J.M., Smith, S.M.: Characterization and propagation of uncertainty in diffusion-weighted MR imaging. *Magnetic Resonance in Medicine* **50** (2003) 1077–1088
- Lenglet, C., Prados, E., Pons, J., Deriche, R., Faugeras, O.: Brain connectivity mapping using Riemannian geometry, control theory and PDEs. *SIAM Journal on Imaging Sciences* **2**(2) (2009) 285–322
- O’Donnell, L., Haker, S., Westin, C.F.: New approaches to estimation of white matter connectivity in diffusion tensor MRI: Elliptic PDEs and geodesics in tensor-warped space. In: *MICCAI 2002*. Volume 2488. (2002) 459–466
- Zalesky, A., Fornito, A.: A DTI-derived measure of cortico-cortical connectivity. *IEEE Transactions on Medical Imaging* **28**(7) (2009) 1023–1036
- Appleton, B., Talbot, H.: Globally minimal surfaces by continuous maximal flows. *IEEE Transactions on Pattern Analysis and Machine Intelligence* **28**(1) (2006) 106–118
- Zach, C., Niethammer, M., Frahm, J.M.: Continuous maximal flows and Wulff shapes: Application to MRFs. In: *CVPR*. (2009) 1911–1918
- Bresson, X., Esedoglu, S., Vandergheynst, P., Thiran, J.P., Osher, S.: Fast global minimization of the active contour/snake model. *Journal of Mathematical Imaging and Vision* **28** (2007) 151–167
- Werlberger, M., Trobin, W., Pock, T., Wedel, A., Cremers, D., Bischof, H.: Anisotropic Huber-L1 optical flow. In: *BMVC*. (2009)
- Boyd, S., Vandenberghe, L.: *Convex Optimization*. Cambridge (2004)
- Arrow, K.J., Hurwicz, L., Uzawa, H.: *Studies in linear and non-linear programming*. Stanford University Press (1958)
- Popov, L.: A modification of the Arrow-Hurwicz method for search of saddle points. *Mathematical Notes* **28**(5) (1980) 845–848
- Pock, T., Cremers, D., Bischof, H., Chambolle, A.: An algorithm for minimizing the Mumford-Shah functional. In: *ICCV*. (2009)
- Behrens, T.E.J., Johansen-Berg, H., Jbabdi, S., Rushworth, M.F.S., Woolrich, M.W.: Probabilistic diffusion tractography with multiple fiber orientations. what can we gain? *NeuroImage* **34**(1) (2007) 144–155